Plasmonic Electro-Optical Switches Operating at Telecom Wavelengths

Jia Hu Zhu · Xu Guang Huang · Xian Mei

Abstract Electro-optical (EO) switches with a subwavelength device length based on metal–dielectric–metal nanocavities waveguide combined with organic EO materials have been proposed and numerically investigated. The finite difference time domain (FDTD) method with perfectly matched layer absorbing boundary condition is adopted to simulate and study their properties. The FDTD simulation results reveal that these structures filled with EO materials can realize the function of switch with low-driving voltage. The wavelength conversion switch structure might become a choice for the design of integrated architectures for optical computing and communication, especially in WDM systems in the nanoscale.

Keywords Surface plasmons · Optical switching devices · Integrated optics devices

Introduction

Surface plasmon polaritons have the potential to guide light at deep subwavelength scale [1, 2]. Therefore, the investigation of plasmonic waveguide structures has been paid great attentions and several different nanoscale plasmonic waveguide structures have been recently proposed, such as metallic nanowires [3, 4], metallic nanoparticle arrays [5, 6] as well as V grooves in metal substrates [7], plasmon slots [8], and metal wedges [9, 10]. Among those structures, waveguides consisted of an insulator sandwiched between two metals serve as metal–dielectric–metal (MDM) waveguides or metal–insulator–metal support propagating surface plasmon modes that are strongly confined in the insulator region with an acceptable propagation length [11]. Therefore, MDM waveguides are promising for the design of nanoscale all-optical devices with a relatively easy fabrication according to the current state of the art [12, 13]. A variety of functional plasmonic MDM structures have been designed and fabricated, such as splitters [14], Y-shaped combiners [15], couplers [16], M–Z interferometers [17, 18], and filters [19–21].

Integrated optical devices and circuits are being increasingly used for light routing and switching in the rapidly developing area of broadband optical communications. Optical switches based on different physical mechanisms with different structures have been proposed [22–25]. Different physical mechanisms can be used to control the refractive index, such as the electro-optical effect [22], the plasma dispersion effect [26], and the thermo-optic effect [27]. Wavelength switch is one of key technologies in fields of optical communication and computing. Especially, in many cases such as WDM systems, it is required to implement several specific wavelengths conversion function. In this letter, a circuit switch and a wavelength conversion switch based on electro-optical effect are proposed and demonstrated numerically by using the finite difference time domain (FDTD) method with perfectly matched layer absorbing boundary condition. An analytic model based on resonator theory is given firstly. The relationship between the peak wavelength and nanocavity length is also addressed. Finally, the characteristics of the circuit switch waveguide structure and the wavelength conversion switch waveguide are analyzed.

J. H. Zhu · X. G. Huang (✉) · X. Mei
Key laboratory of Photonic Information Technology of
Guangdong Higher Education Institutes,
South China Normal University,
Guangzhou 510006, China
e-mail: huangxg@scnu.edu.cn

Nanocavity Theory Model

Figure 1a shows the structure schematic of the nanocavity composed of two wide waveguides and a narrow waveguide filled with SiO$_2$ material. Obviously, the structure can be treated as two MDM waveguides with different widths. Because the width of the narrow MDM waveguide is much smaller than that of the wide MDM waveguide, here we call the narrower waveguide as nanocavity. The dielectric

constant ε_m of silver can be calculated based on Drude–Lorentzian model:

$$\varepsilon_m(\omega) = \varepsilon_\infty - \frac{\omega_D^2}{\omega^2 + i\gamma_D\omega} - \sum_{m=1}^{2} \frac{g_{Lm}\omega_{Lm}^2 \Delta\varepsilon}{\omega^2 - \omega_{Lm}^2 + i2\gamma_{Lm}\omega}, \quad (1)$$

where, ε_∞=2.3646, ω_D=8.7377 eV, γ_D=0.07489 eV, $\Delta\varepsilon$= 1.1831, g_{L1}=0.26663, ω_{L1}=4.3802 eV, γ_{L1}=0.28 eV, g_{L2}= 0.7337, ω_{L2}=5.183 eV, and γ_{L2}=0.5482 eV. Equation 1

Fig. 1 a Schematics of MDM nanocavity structures (colored). b The electric fields on the two reflection surfaces. c The schematics of estimating the value of t. d and e The space distributions of the mode
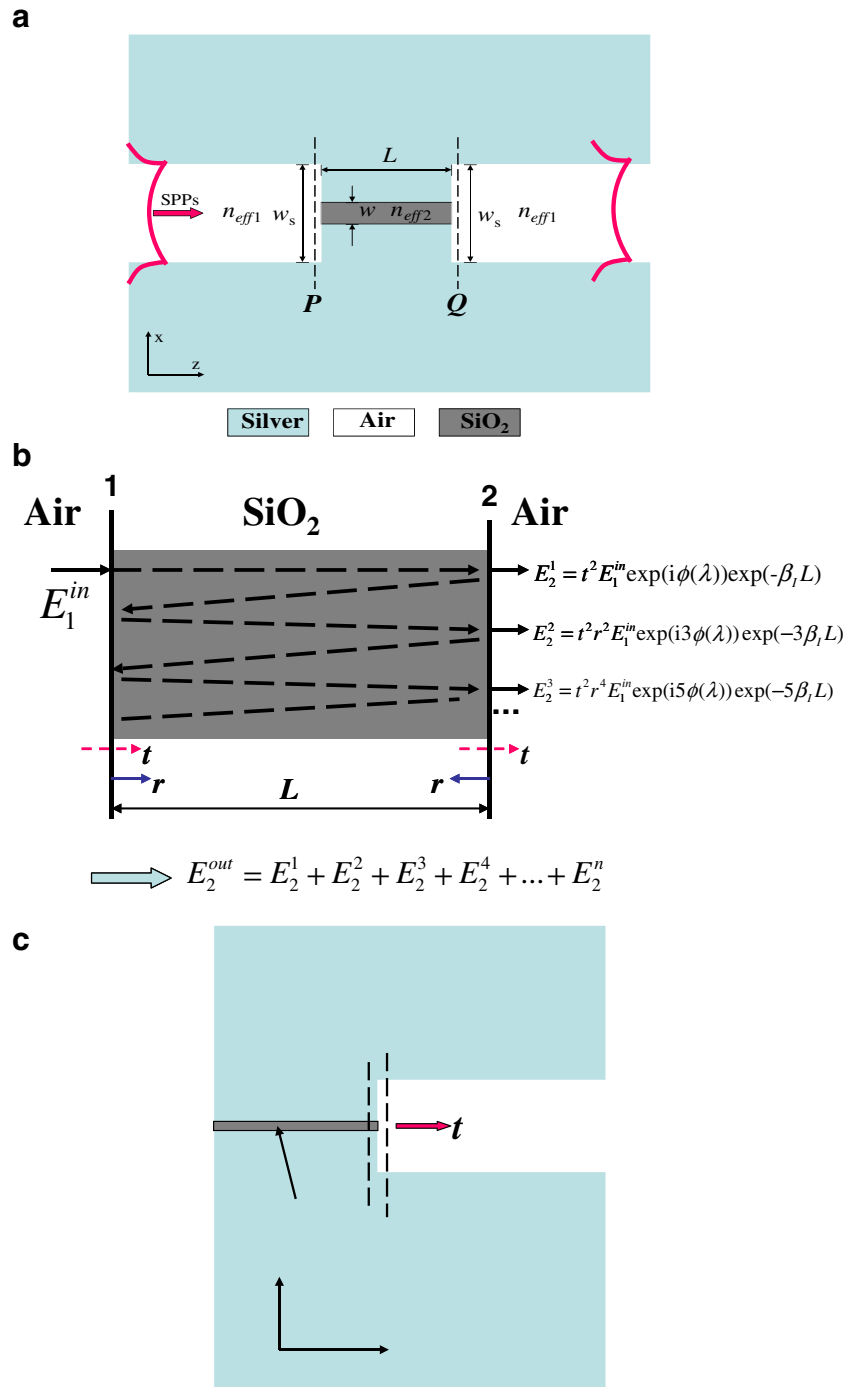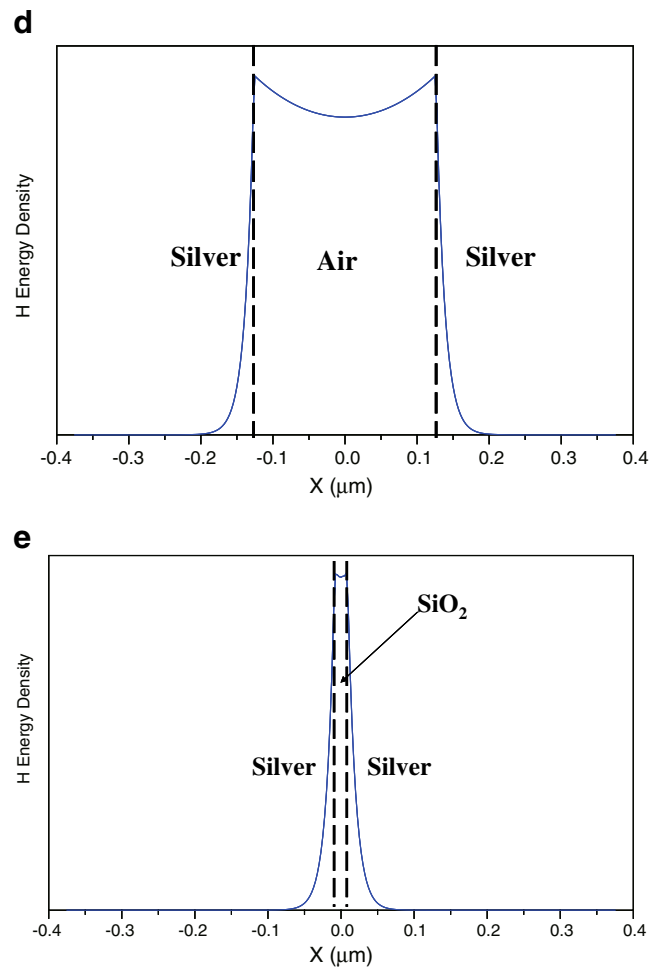
Fig. 1 (continued)

gives a good description of empirical dielectric constant data for silver within the range of 500–1,800 nm [28]. The complex propagation constant $\beta = \beta_R + j\beta_I$ of surface plasmon polaritons in every MDM waveguide can be obtained by solving the dispersive mode equation [13, 29]:

$$\varepsilon_D k_{z2} + \varepsilon_m k_{z1} \tanh\left(-\frac{ik_{z1}}{2}w\right) = 0, \qquad (2)$$

k_{z1} and k_{z2} defined as: $k_{z1}^2 = \varepsilon_D k_0^2 - \beta^2$ and $k_{z2}^2 = \varepsilon_m k_0^2 - \beta^2$, where ε_D and ε_m are, respectively, dielectric constants of the dielectric and the metal. $k_0 = 2\pi/\lambda$ is the wave number of light with wavelength λ in vacuum. w is the width of the slit waveguide. The effective index is represented as $n_{\text{eff}} = \beta_R/k_0$.

The effective index of the waveguide decreases with the increasing of the width of waveguide w at the same wavelength [20]. Therefore, the effective index n_{eff2} of the nanocavity part can be larger than n_{eff1} of the wide MDM waveguide part due to the difference of the width of the two waveguides and mediums filled in. The wave transmitted into the nanocavity will be partly reflected at two ends of the nanocavity, because of the index differences between n_{eff2}

and n_{eff1}. Therefore, one can expect the nanocavity operates as a Fabre–Pérot resonator. Figure 1b shows the electric fields on the two reflection ends of the nanocavity. r and t are respectively the reflection and transmission coefficients of an incident beam in the structure. And E_1^{in} and E_2^{out} stand for the fields of incident and output beams, respectively. Based on Fabre–Pérot resonator properties, one has $E_2^{\text{out}} = E_2^1 + E_2^2 + E_2^3 + E_2^4 + \ldots + E_2^n$(shown in Fig. 1b). The transmitted electric fields at end 2 of E_2^1, E_2^2 and E_2^3 are respectively given as follows:

$$E_2^1 = t^2 E_1^{\text{in}} \exp(i\phi(\lambda)) \exp(-\beta_I L), \qquad (3)$$

$$E_2^2 = t^2 r^2 E_1^{\text{in}} \exp(i3\phi(\lambda)) \exp(-3\beta_I L), \qquad (4)$$

$$E_2^3 = t^2 r^4 E_1^{\text{in}} \exp(i5\phi(\lambda)) \exp(-5\beta_I L), \qquad (5)$$

here the phase delay is $\phi(\lambda) = (2\pi/\lambda)n_{\text{eff}} \cdot L + \varphi_1 + \varphi_2$, where φ_1 and φ_2 are, respectively, the phase shifts of the beam reflected at both ends of the nanocavity. β_I and L

stand for the imaginary part of the propagation constant and the length of the nanocavity, respectively. Therefore, one has the total output electric field of E_2^{out}:

$$
\begin{aligned}
E_2^{\mathrm{out}} &= t^2 E_1^{\mathrm{in}} \exp(i\phi(\lambda)) \exp(-\beta_I L) + \\
&\quad t^2 r^2 E_1^{\mathrm{in}} \exp(i3\phi(\lambda)) \exp(-3\beta_I L) + \\
&\quad t^2 r^4 E_1^{\mathrm{in}} \exp(i5\phi(\lambda)) \exp(-5\beta_I L) + . \\
&\quad \dots \\
&= \frac{t^2 E_1^{\mathrm{in}} \exp(i\phi(\lambda)) \exp(-\beta_I L)}{1 - r^2 \exp(i2\phi(\lambda)) \exp(-2\beta_I L)}
\end{aligned} \tag{6}
$$

Therefore, the transmittance T is given by

$$
\begin{aligned}
T &= \left| \frac{E_2^{\mathrm{out}}}{E_1^{\mathrm{in}}} \right|^2 = \left| \frac{t^2 \exp(i\phi(\lambda)) \exp(-\beta_I L)}{1 - r^2 \exp(i2\phi(\lambda)) \exp(-2\beta_I L)} \right| \\
&= \frac{t^4 \exp(-2\beta_I L)}{1 + r^4 \exp(-4\beta_I L) - 2r^2 \exp(-2\beta_I L) \cos(2\phi(\lambda))}
\end{aligned} \tag{7}
$$

It can be seen from Eq. 7 that the transmittance T will become maximum, only when the following condition is satisfied: $2\phi(\lambda) = 2m\pi (m=1, 2, 3\dots)$. Therefore, the peak wavelength $\lambda_{\max}$ of the nanocavity structure is determined as follows:

$$
\lambda_{\max} = 2n_{\mathrm{eff}} L / (m - (\varphi_1 + \varphi_2)/(2\pi)). \tag{8}
$$

From Eq. 8, one can see that the wavelength $\lambda_{\max}$ is proportional to the length and the effective index of the nanocavity, respectively. The maximum transmittance T can be expressed as follows:

$$
T_{\max} = \frac{t^4 \exp(-2\beta_I L)}{[1 - r^2 \exp(-2\beta_I L)]^2}. \tag{9}
$$

Obviously, the maximum transmittance $T_{\max}$ is determined by the reflection coefficient of r and transmission coefficient of t, as well as propagation loss of $\exp(-2\beta_I L)$. Provided that $r^2 + t^2 = 1$ and propagation loss of $\exp(-2\beta_I L) = 0$, one would obtain the highest transmittance $T_{\max}=1$.

On the other hand, if the following condition is satisfied: $2\phi(\lambda) = (2m + 1)\pi$, the transmittance T will become minimum. The minimum transmittance T is given as follows:

$$
T_{\min} = \frac{t^4 \exp(-2\beta_I L)}{[1 + r^2 \exp(-2\beta_I L)]^2}. \tag{10}
$$

It can be seen from Eq. 10 that $T_{\min}=0$ only when the propagation loss of $\exp(-2\beta_I L)$ can be ignored.

In order to estimate values of $T_{\max}$ and $T_{\min}$, it is necessary to know the values of β_I and t (or r). For a slit waveguide with a small width of w, solving Eq. 2 gives n_{eff} and β_I. Figure 1c shows the calculation of the value of t. One unit incident optical power signal from point S transmits along the waveguide. The power monitor is set at the position of P which is about 10 nm away from point S, to detect the transmitted power P_t. Therefore, the value of t is equal to P_t.

Take nanocavity structure (shown in Fig. 1a) with $w_s = 250$ nm, $w=15$ nm, and $L=150$ nm as an example, the values of n_{eff} and β_I are respectively calculated to be 2.99 and 0.17. The value of t is calculated to be 0.2. Thus, the peak wavelength of $\lambda_{\max} \approx 900$ nm for $m=1$ and $\varphi_1 = \varphi_2 = 0$, while the maximum transmittance of $T_{\max}$ is simply estimated to be 66% according to the Eq. 9, namely, the insertion loss is about -1.8 dB. According to Eq. 10, the minimum transmittance of $T_{\min}$ could be theoretically calculated to be 0.012, namely, the extinction ratio of the nanocavity structure as a wavelength shift switch will be aroud -19.1 dB.

The refractive index of SiO_2 is set to be 1.44. In the following FDTD simulations, the grid sizes in the x and z directions are set to be 3×3 nm. The fundamental transverse magnetic (TM) mode of the plasmonic waveguide is launched from the left to the right of the waveguide. Because the width of the MDM plasmonic waveguide is much smaller than the wavelength, only the fundamental TM waveguide mode can propagate. Two power monitors are set at the locations of P (outside the resonator but just near its entrance) and Q (outside the resonator but just near its exit) to detect the incident power without reflection (replacing narrow waveguide with wide waveguide) and transmitted power of P_{in} and P_{out}. The transmittance is defined to be $T=P_{\mathrm{out}}/P_{\mathrm{in}}$. The space distributions of the modes are presented in Fig. 1d and e. For the sake of comparison, the wide waveguide width of w_s, the nanocavity waveguide width of w, the distance of d, and the nanocavity waveguide length of L are kept the same as the above theoretical analysis, namely, respectively fixed to be 250, 15, 50, and 150 nm. A typical selective filtering transmission spectrum is shown in Fig. 2a. From Fig. 2a, one can see that the peak wavelength occurs at around the wavelength of 910 nm and its transmittance is about 64%, which agree with the above theoretical analysis well. The inset of Fig. 2a shows the peak wavelength as a function of the nanocavity length L. From it, it can be seen that the peak wavelength linearly increases with the increase of the length of the nanocavity as expected from Eq. 8. The selective wavelength can be easily tuned by choosing an appropriate nanocavity length. The spectrum of the nanocavity structure in a log scale is shown in Fig. 2b. It shows that the insertion loss of this filter is about -1.9 dB as expected from Eq. 9. The extinction ratio of the nanocavity is about -20 dB as expected from Eq. 10. Therefore, the simulated results agree with the theoretical analysis well.

Discussion of Dual-Nanocavities Structure for Circuit Switch

Figure 3 shows a typical schematic of a 1×2 circuit switch structure based on MDM nanocavities. The electro-optical
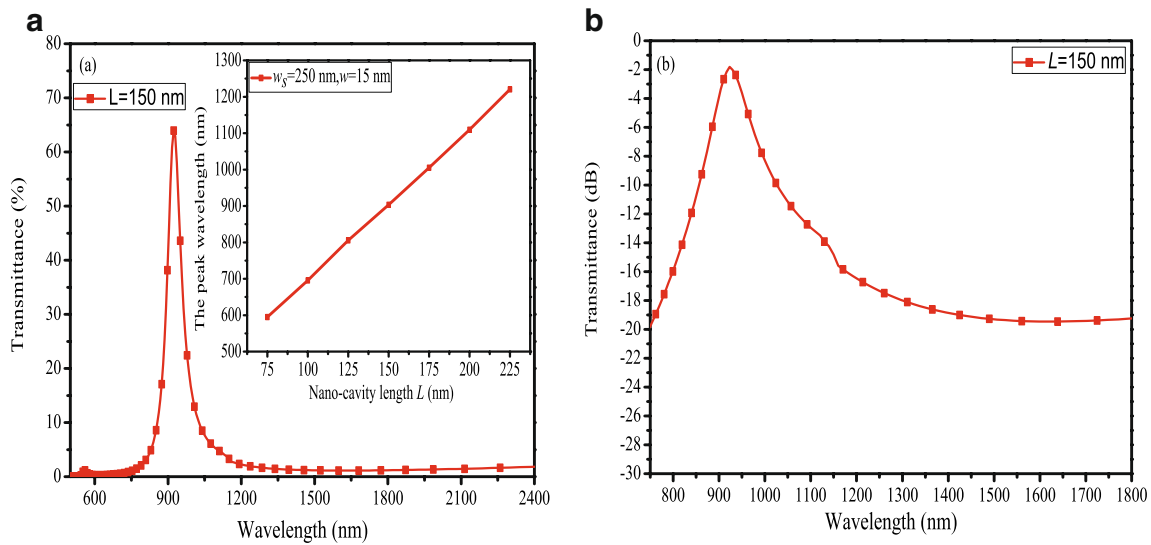
Fig. 2 **a** Transmission spectrum of the nanocavity structure with the length of $L=150$ nm. Transmission spectra versus the nanocavity length L with the same width of $w=15$ nm (*inset*). **b** The spectrum of the nanocavity structure in a log scale

(EO) material, an organic material with the refractive index of 2.2, filled into the nanocavities of the channels 1 and 2 is assumed to be 4-dimethylamino-N-methyl-4-stilbazolium tosylate. It exhibits a large EO coefficient ($dn/dE=3.41$ nm/V) compared with that of standard inorganic EO materials such as LiNbO3 ($dn/dE=0.16$ nm$V$), because of a large delocalised π electron system [30]. Two power monitors are set at the locations of Q_1 and Q_2 (outside the resonator but just near its exit) to detect the output channels 1 and 2 transmitted powers of P_1 and P_2. The transmittance are defined to be $T_1=P_1/P_{in}$ and $T_2=P_2/P_{in}$, where P_{in} is the

incident power without reflection of the beam. L_1 and L_2 are respectively the nanocavity length of the channels 1 and 2. The others parameters of the structure are kept the same as Section Nanocavity Theory Model. An electric field is added in order to control the refractive index of EO material.

Figure 4a shows transmission spectra at the outputs of the two channels. One can see that channels 1 and 2 and respectively select 1,280 and 1,550 nm bands with the length of $L_1=120$ nm and $L_2=142$ nm, and the maximum transmittance in two bands can exceed 30% (−5.2 dB). Figure 4b shows transmission spectra at the outputs of the two channels after an eclectic field ($V=1.95$ V, and the electric field intensity correspond to 0.13 KV/μm which is acceptable experimentally) is applied. One can see that channels 1 and 2 can respectively select 1,550 and 1,860 nm bands with the length of $L_1=120$ nm and $L_2=142$ nm. From Fig. 4a and b, one can see that the peak wavelength shift toward long wavelength after the electric field applied. It is noticed that the output wavelength at 1,550 nm can be switched from the channels 2 to 1 when the applied voltage is tuned from $V=0$ to 1.95 V. Insertion loss is defined as the ratio between the output and input power. The insertion losses of the channels 1 and 2 are respectively −3.6 and −5.1 dB for 1,550 nm wavelength. Isolation is defined as the output power ratio between two separate channels. The isolation is about 18 dB between channels 1 and 2 for 1,550 nm wavelength at the absence of electric field. Extinction ratio is defined as insertion loss difference between the input and output ports in the states on and off. The extinction ratio of the channels 1 and 2 are
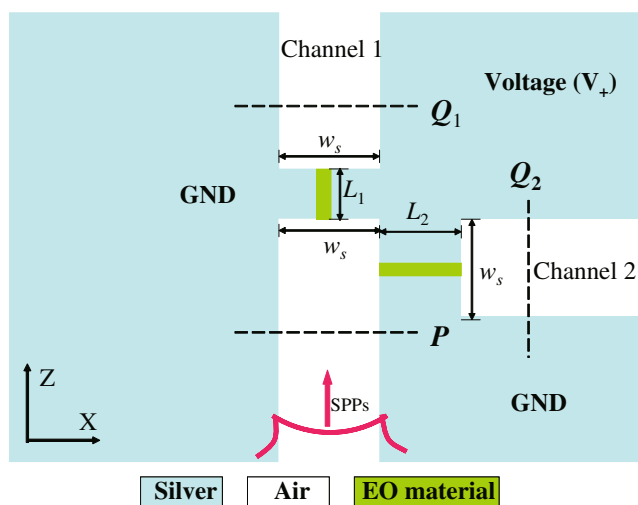

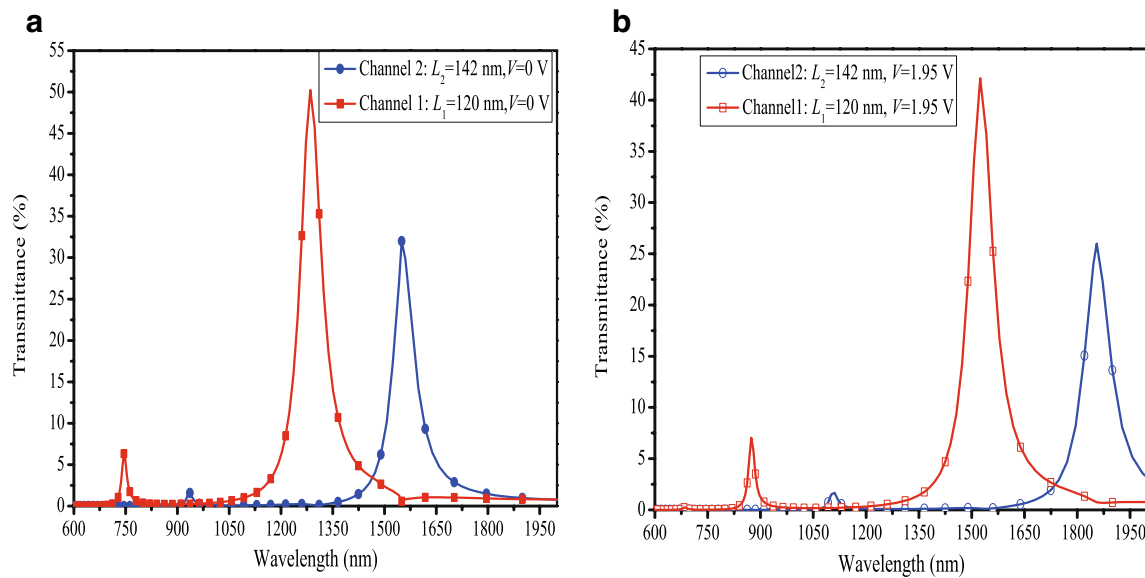**Fig. 3** Schematic of 1×2 circuit switch structure based on MDM nanocavities (*colored*)

Fig. 4 **a** Transmission spectra of the 1×2 circuit switch structure in the absence of electric field with the lengths of $L_1=120$ and $L_2=142$ nm (*colored*). **b** Transmission spectra of the 1×2 circuit switch structure in the presence of electric field ($V=1.95$ V) with the lengths of $L_1=120$ and $L_2=142$ nm
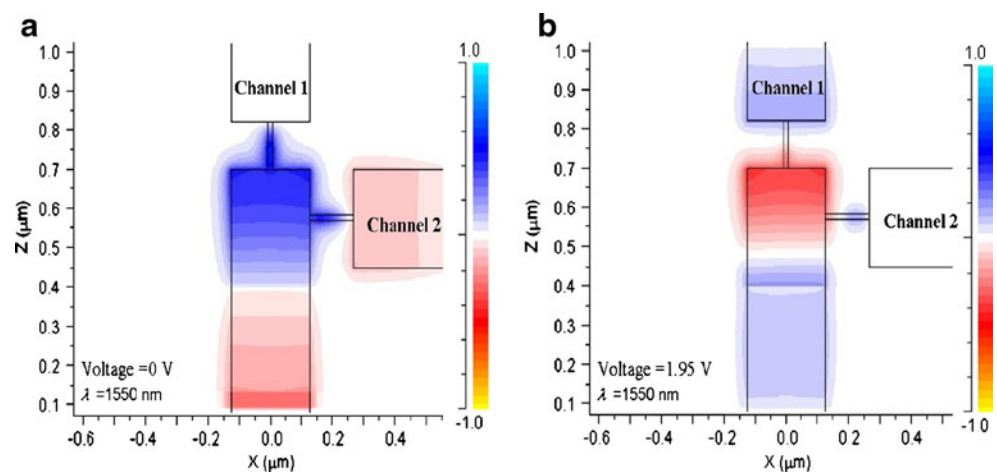
respectively about 18 and 24 dB for 1,550 nm wavelength. From the inset of Fig. 2a, one can see that the switch wavelength can be easily tuned by choosing an appropriate nanocavity length. Therefore, this structure is suitable for wideband wavelengths switch.

Figure 5a and b show the propagation of field H_y for a monochromatic wave with wavelength of 1,550 nm launched into circuit switch structure. The switch effect is clearly observed. From the figure, one can see the wave with wavelength of 1,550 nm is output through the channel 2 in the absence of electric filed shown in Fig. 5a and output through the channel 1 in the presence of electric filed ($V=1.95$ V) shown in Fig. 5b.

Discussion of Dual-Nanocavities Structure for Wavelength Conversion Switch

Figure 6 shows a typical schematic of a 1×2 wavelength conversion switch structure based on MDM nanocavities. Two power monitors are set at the locations of Q_1 and Q_2 (outside the resonator but just near its exit) to detect the output channels 1 and 2 transmitted powers of P_1 and P_2. The transmittance are defined to be $T_1=P_1/P_{in}$ and $T_2=P_2/P_{in}$, where P_{in} is the incident power without reflection of the beam. L_1 and L_2 are respectively the nanocavity length of the channels 1 and 2. The others parameters of the structure are kept the same as Section Nanocavity Theory

Fig. 5 The contour profiles of field Hy of the 1×2 circuit switch structure at wavelength λ=1,550 nm (*colored*). All parameters of the structure are same as in Fig. 4

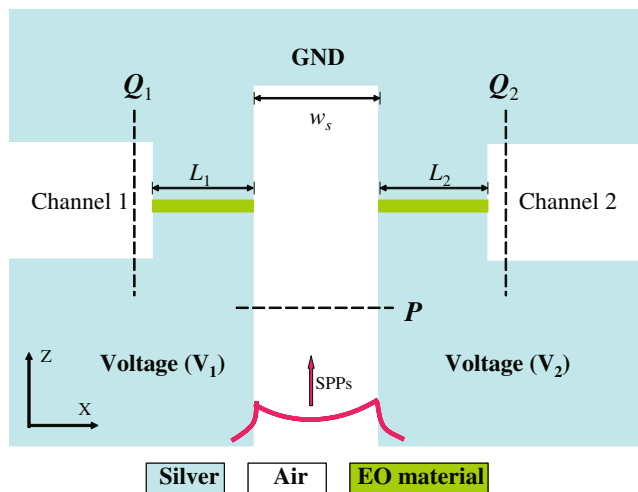**Fig. 6** Schematic of 1×2 wavelength conversion switch structure based on MDM nanocavities (*colored*)

2 to 1 when the applied voltages are tuned synchronously from $V_1=0$ to 1.8 V and $V_2=1.8$ to 0 V. And the output wavelength at 1,310 nm can be switched from channels 1 to 2 when the applied voltage is tuned synchronously from $V_1=0$ to 1.8 V and $V_2=1.8$ to 0 V Therefore, the waveguide structure is a typical wavelengths conversion switch structure. The insertion losses of both channels 1 and 2 are −5.7 and −6.8 dB for 1,310 and 1,550 nm wavelength, respectively. The extinction ratio of both channels 1 and 2 are respectively about 16 dB for 1,550 nm wavelength and 23 dB for 1,310 nm wavelength. Cross-talk is defined as the ratio between the power of the undesired and desired bands at the outputs. The cross-talk between channels 1 and 2 is around −23 dB for the 1,550 nm wavelength, and the cross-talk between them is −28 dB for the 1,310 nm wavelength. Based on electro-optical effect, the switching time is about several nanoseconds level.

Model. V_1 and V_2 are respectively voltages of the channels 1 and 2.

Figure 7a shows transmission spectra at the outputs of the two channels with the voltage of $V_1=0$ V and $V_2=1.8$ V. One can see that channels 1 and 2 can respectively select 1,310 and 1,550 nm bands with the length of $L_1=L_2=$ 120 nm Fig. 7b shows transmission spectra at the outputs of the two channels with the voltage of $V_1=1.8$ V and $V_2=0$ V. One can see that channels 1 and 2 can respectively select 1,550 and 1,310 nm bands with the length of $L_1=L_2=$ 120 nm. From Fig. 7a and b, it is noticed that the output wavelength at 1,550 nm can be switched from the channels

Conclusion

In conclusion, we demonstrate electro-optic switches with a subwavelength device length based on MDM nanocavities waveguide combined with organic EO materials. The circuit switch and wavelength conversion switch are introduced and their performances are analyzed. The structure is suitable for wideband wavelengths switch. The wavelength conversion switch structure might become a choice for the design of integrated architectures for optical computing and communication, especially in WDM systems in the nanoscale.
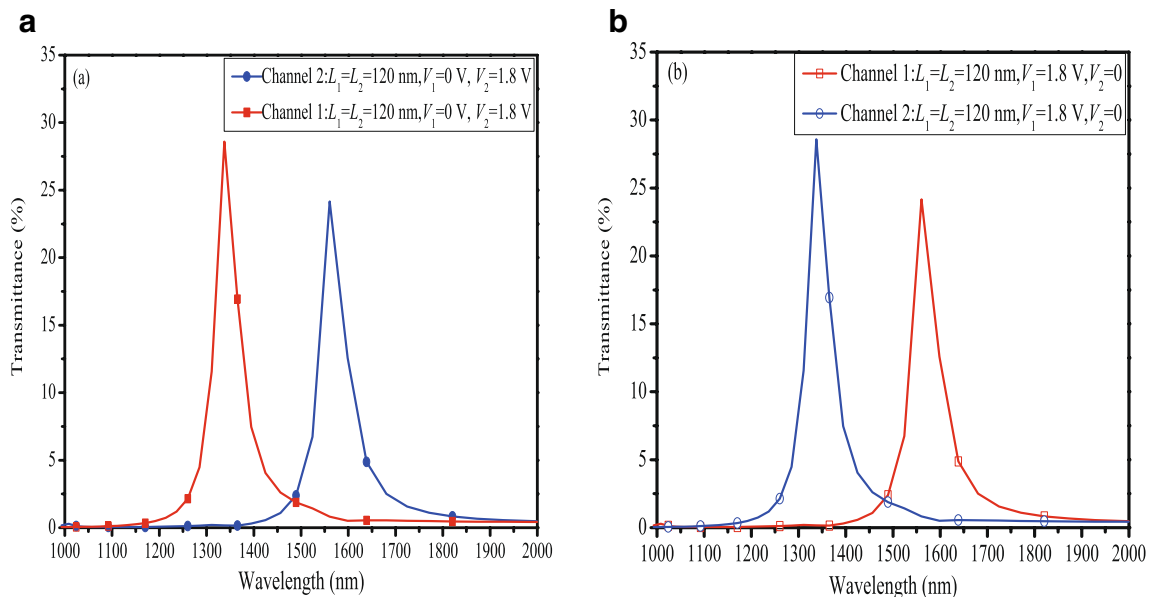

Fig. 7 a Transmission spectra of the 1×2 wavelengths conversion switch structure with the lengths of $L_1=L_2=120$ nm, $V_1=0$ V and $V_2=1.8$ V (*colored*). **b** Transmission spectra of the 1×2 wavelengths conversion switch structure with the lengths of $L_1=L_2=120$ nm, $V_1=1.8$ V and $V_2=0$ V

References

1. Raether H (1998) Surface plasmon on smooth and rough surfaces and gratings. Springer, Berlin, Germany
2. Liu L, Han Z, He S (2005) Novel surface plasmon waveguide for high integration. Opt Express 13(17):6445–6650
3. Weeber JC, Dereu A, Griard C, Krenn JR, Goudonnet JP (1999) Plasmon polaritons of metallic nanowires for controlling submicron propagation of light. Phys Rev B 60(12):9061–9068
4. Dickson RM, Lyon LA (2000) Unidirectional plasmon propagation in metallic nanowires. J Phys Chem B 104(26):6095–6098
5. Quinten M, Leitner A, Krenn JR, Aussenegg FR (1998) Electromagnetic energy transport via linear chains of silver nanoparticles. Opt Lett 23(17):1331–1333
6. Maier SA, Kik PG, Atwater HA, Meltzer S, Harel E, Koel BE, Requicha AAG (2003) Local detection of electromagnetic energy transport below the diffraction limit in metal nanoparticle plasmon waveguides. Nat Mater 2(4):229–232
7. Bozhevolnyi SI, Volkov VS, Devaux E, Ebbesen TW (2005) Channel plasmon-polariton guiding by subwavelength metal grooves. Phys Rev Lett 95:046802
8. Liu L, Han Z, He S (2005) Novel surface plasmon waveguide for high integration. Opt Express 13:6645–6650
9. Moreno E, Rodrigo SG, Bozhevolnyi SI, Martin-Moreno L, Garcia-Vidal FJ (2008) Guiding and focusing of electromagnetic fields with wedge plasmon polaritons. Phys Rev Lett 100:023901
10. Boltasseva A, Volkov VS, Nielsen RB, Moreno E, Rodrigo SG, Bozhevolnyi SI (2008) Triangular metal wedges for subwavelength plasmon-polariton guiding at telecom wavelength. Opt Express 16:5252–5260
11. Veronis G, Yu Z, Kocabas SE, Miller DAB, Brongersma ML, Fan S (2009) Metal-dielectric-metal plasmonic waveguide devices for manipulating light at the nanoscale. Chin Opt Lett 7:302–308
12. Neutens P, Dorpe PV, Vlaminck ID, Lagae L, Borghs G (2009) Electrical detection of confined gap plasmons in metal–insulator–metal waveguides. Nature Photonics 3:283–286
13. Dionne JA, Sweatlock LA, Atwater HA (2006) Plasmon slot waveguides: towards chip-scale propagation with subwavelength scale localization. Phys Rev B 73:035407
14. Veronis G, Fan S (2005) Bends and splitters in metal–dielectric–metal subwavelength plasmonic waveguides. Appl Phys Lett 87:131102
15. Gao H, Shi H, Wang C, Du C, Luo X, Deng Q, Lv Y, Lin X, Yao H (2005) Surface plasmon polariton propagation and combination in Y-shaped metallic channels. Opt Express 13:10795–10800
16. Zhao H, Huang X, Huang J (2008) Novel optical directional coupler based on surface plasmon polaritons. Physica E 40:3025–3029
17. Wang B, Wang G (2004) Surface plasmon polariton propagation in nanoscale metal gap waveguides. Opt Lett 29:1992–1994
18. Han Z, Liu L, Forsberg E (2006) Ultra-compact directional couplers and Mach–Zehnder interferometers employing surface plasmon polaritons. Opt Commun 259:690–695
19. Zhang Q, Huang X-G, Lin X-S, Tao J, Jin X-P (2009) A subwavelength coupler-type MIM optical filter. Opt Express 17(9):7549–7554
20. Lin X-S, Huang X-G (2008) Tooth-shaped plasmonic waveguide filters with nanometeric sizes. Opt Lett 33(23):2874–2876
21. Lin X-S, Huang X-G (2009) Numerical modeling of a teeth-shaped nanoplasmonic waveguide filter. J Opt Soc Am B 26(7):1263–1268
22. Zhang A, Chan KT, Demokan MS et al (2005) Integrated crystal optical switch based on total internal reflection. Appl Phys Lett 86:211108
23. Min CJ, Veronis G (2009) Absorption switches in metal–dielectric–metal plasmonic waveguides effective index. Opt Express 17(13):10757–10766
24. Yu ZF, Veronis G, Fan SH (2008) Gain-induced switching in metal–dielectric–metal plasmonic waveguides. Appl Phys Lett 92:041117
25. Min CJ, Wang P, Chen CC, Deng Y et al (2008) All-optical switching in subwavelength metallic grating structure containing nonlinear optical material. Opt Lett 33(8):869–871
26. Li B, Chua S-J (2001) 2×2 optical waveguide switch with bow-tie electrode based on carrier-injection total internal reflection in SiGe alloy. IEEE Photonics Technol Lett 13:206
27. Diemeer MBJ, Brons JJ, Trommel ES (1989) Polymeric optical waveguide switch using the thermooptic effect. J Lightwave Technol 7:449
28. Johnson PB, Christy RW (1972) Optical constants of the noble metals. Phys Rev 6:4370–4379
29. Boltasseva A, Bozhevolnyi SI, Nikolajsen T, Leosson K (2006) Compact Bragg gratings for long-range surface plasmon polaritons. J Lightwave Technol 24:912–918
30. Geis W, Sinta R, Mowers W, Deneault SJ, Marchant MF, Krohn KE, Spector SJ, Calawa DR, Lyszczarz TM (2004) Fabrication of crystalline organic waveguides with an exceptionally large electro-optic coefficient. Appl Phys Lett 84:3729–3731